HHS Public Access

Author manuscript

Nat Cell Biol. Author manuscript; available in PMC 2015 March 01.

Published in final edited form as:

Nat Cell Biol. 2014 September ; 16(9): 841–851. doi:10.1038/ncb3029.

Prostaglandin signaling regulates ciliogenesis by modulating intraflagellar transport

Daqing Jin[1], **Terri T. Ni**[2], **Jianjian Sun**[1], **Haiyan Wan**[2], **Jeffrey D. Amack**[4], **Guangju Yu**[1], **Jonathan Fleming**[3], **Chin Chiang**[3], **Wenyan Li**[1], **Anna Papierniak**[5], **Satish Cheepala**[6], **Gwenaëlle Conseil**[7], **Susan P.C. Cole**[7], **Bin Zhou**[8], **Iain A. Drummond**[9], **John D. Schuetz**[6], **Jarema Malicki**[5], and **Tao P. Zhong**[1,2,*]

[1]State Key Laboratory of Genetic Engineering, Department of Genetics, Fudan University School of Life Sciences, Shanghai 200433, China

[2]Department of Medicine, Vanderbilt University School of Medicine, TN37232, USA

[3]Department of Cell & Developmental Biology, Vanderbilt University School of Medicine, TN37232, USA

[4]Department of Cell & Developmental Biology, State University of New York Upstate Medical University, NY13210, USA

[5]MRC Center for Developmental and Biomedical Genetics, The University of Sheffield, Sheffield, United Kingdom

[6]Department of Pharmaceutical Science, St. Jude Children's Research Hospital, TN38163, USA

[7]Division of Cancer Biology and Genetics, Queen's University, Kingston, ON K7L3N6, Canada

[8]Institute for Nutritional Sciences, Chinese Academy of Sciences, Shanghai, 200031, China

[9]Department of Medicine, Massachusetts General Hospital, Harvard Medical School, MA 02148, USA

Abstract

Cilia are microtubule-based organelles that mediate signal transduction in a variety of tissues. Despite their importance, the signaling cascades that regulate cilia formation remain incompletely

*Correspondence should be addressed to: T. P. Z. (taozhong@fudan.edu.cn).

Author Contributions

T.P.Z. conceived and directed the project. T.T.N. and H.W. initiated the project and discovered the *lkt* gene as ABCC4. D.J. performed most experiments and discovered the roles of COX, ABCC4 and EP4 in ciliogenesis. J.J.S. and G.Y. conducted cell culture experiments. J.D.A. performed KV flow experiments. G.C. and J.D.S. conducted PGE_2 efflux experiments. J.F., C.C. and B.Z. performed part of cell culture experiments. G.C. and S.P.P.C. carried out vesicular transport assays. W.L. conducted double in situ hybridization. A.P. and J.M. tested roles of PGE_2 in *ift* mutants and involved in early mutant analyses. I.A.D. performed histology and provided reagents. T.P.Z., D.J., J.M prepared figures and wrote the paper.

Competing Financial Interests

The authors declare no competing financial interests.

Accession numbers

GenBank: *lkt/abcc4*, EU586042.

understood. Here we report that prostaglandin signaling affects ciliogenesis by regulating anterograde intraflagellar transport (IFT). Zebrafish *leakytail* (*lkt*) mutants display ciliogenesis defects, and *lkt* locus encodes an ATP-binding cassette transporter (ABCC4). We show that Lkt/ABCC4 localizes to the cell membrane and exports prostaglandin E_2 (PGE_2), a function that is abrogated by the Lkt/ABCC4^{T804M} mutant. PGE_2 synthesis enzyme Cyclooxygenase-1 and its receptor, EP4, which localizes to the cilium and activates cAMP-mediated signaling cascade, are required for cilia formation and elongation. Importantly, PGE_2 signaling increases anterograde but not retrograde velocity of IFT and promotes ciliogenesis in mammalian cells. These findings lead us to propose that Lkt/ABCC4-mediated PGE_2 signaling acts through a ciliary G-protein-coupled receptor, EP4, to upregulate cAMP synthesis and increase anterograde IFT, thereby promoting ciliogenesis.

INTRODUCTION

In mammals, prostaglandins (PGs) regulate a wide variety of important physiological processes, including pain perception and body temperature, cardiovascular homeostasis, reproduction, and cancer progression[1, 2]. The prostaglandin precursor PGH_2 is synthesized by COX-1 and COX-2 in the endoplasmic reticulum from arachidonic acid, a 20-carbon polyunsaturated fatty acid released from membrane phospholipids[1]. COX-1 serves a homeostatic function and is responsible for basal, constitutive prostaglandin synthesis, whereas COX-2 increases production of prostaglandins during inflammatory response and in cancer[1]. The PG precursor is metabolized by prostaglandin synthases to form structurally related, bioactive prostanoids in various tissues, including PGE_2, PGD_2, PGF2α PGI_2 and Thromboxane A_2 (TxA_2)[1]. PGE_2 functions through activation of G-protein-coupled receptors (GPCRs), including EP1 through EP4. Among them, EP2 and EP4 increase the intracellular cyclic adenosine monophosphate (cAMP) and activate protein kinase A (PKA) signaling[1, 3]. Although prostaglandins have important functions in a variety of physiological and pathological processes, their roles in ciliogenesis have not been previously investigated and remain virtually unknown.

Cilia are formed and extended by IFT, which transports cargo proteins along microtubules from the base to the tip of the cilium and back to the cell body. This process is mediated by kinesins in the anterograde direction and by cytoplasmic dynein motor in the retrograde direction[4, 5]. Basal body proteins are also essential for cilia formation. They anchor the cilium at the cell surface, provide template for microtubules in the ciliary axoneme, and serve as a relay station for protein and lipid traffic from the Golgi complex to the ciliary membrane[6, 7]. Ciliary dysfunction causes multisystemic genetic disorders commonly known as human ciliopathies[5, 8].

Many developmental pathways have been shown to function in ciliogenesis[4, 5]. Fibroblast growth factor (FGF) signalling regulates cilia length and function through ciliogenic transcription factor Foxj1 in diverse epithelia[9]. In zebrafish Kupffer's vesicle (KV), both Wnt/β-catenin and Notch pathway regulate Foxj1 expression and controls ciliogenesis[10, 11]. Components of the phosphatidylinositol signaling cascade also regulate cilia formation in zebrafish. This conclusion is based on observations that knockdown of inositol-

pentakisphosphate 2-kinase (Ipk1) reduced cilia length and decreased the cilia beating frequency[12]. Our understanding of ciliogenesis regulation is, however, incomplete. Using zebrafish genetics and cultured human epithelial cells we reveal for the first time the roles of prostaglandin signaling in vertebrate ciliogenesis.

RESULTS

leakytail mutants display defective ciliogenesis

In the course of a zebrafish genetic screen for mutations that affect organogenesis, we identified the *leakytail* (*lkt*) mutant that displayed randomized heart looping (Fig. 1g–i), as well as cilia-associated phenotypes, including ventrally curved body axis (Fig. 1a, b), hydrocephalus (Fig. 1c, d), abnormal otolith number (Fig. 1e, f), and laterality defects of the brain and other organs (Supplementary Fig. S1a–d, g). Randomized expression of a nodal-related gene *southpaw* (*spaw*)[13] and a nodal target gene *pitx2*[13] occurred in the lateral plate mesoderm (Fig. 1v, w; Supplementary Fig. 1h). To test roles of *lkt* in ciliogenesis, we visualized cilia formation in developing embryos. At 24 hour post-fertilization (hpf), zebrafish otic vesicles (OVs) contain two clusters of long tether cilia and many short cilia distributed throughout OVs (Fig. 1j). In contrast to wild-type OVs (Fig. 1j), mutant OVs lacked short cilia but had relatively normal tether cilia (Fig. 1k). At 96 hpf, cristae kinocilia in ear semicircular canals were lost in *lkt* mutants (Fig. 1l, m). In Kupffer's vesicle (KV), we observed cilia loss and length reduction in mutant embryos relative to wild-type (Fig. 1n, o; r, s). *lkt* mutants also exhibited a loss of ependymal cell cilia in the spinal canal (Fig. 1p, q). However, *lkt* mutants do not form kidney cysts (Fig. 1t, u), and the formation and growth of pronephric cilia are not affected in *lkt* mutants either (Supplementary Fig. 1e, f).

leakytail locus encodes the ABCC4 transporter

To determine the molecular underpinnings of *lkt* ciliopathy, we mapped *lkt* to chromosome 6 of the zebrafish genome using whole genome bulk segregant analyses (Fig. 2a)[14]. Subsequent fine mapping refined *lkt* genetic interval to a single bacterial artificial chromosomal clone (BAC) (Fig. 2a). One of four transcribed regions on this BAC encodes ABCC4 (Mrp4), a subfamily 'C' member of the ATP-binding cassette (ABC) superfamily of transport proteins (Fig. 2a, b)[15–17]. At the amino acid level, zebrafish Lkt/ABCC4 is 68.5% identical to the human ABCC4 transporter (Supplementary Fig. 2), with a high degree of conservation in transmembrane (TM) domains and nucleotide binding domains (NBD)[18] critical for normal ABC transporter function (Fig. 2b; Supplementary Fig. 2). Sequencing of *abcc4* from *lkt* mutants identified a threonine to methionine substitution at position 804 (T804M) (Fig. 2b, c). This threonine localizes to the third cytoplasmic loop of the *lkt* polypeptide and is evolutionarily conserved from *Drosophila* to human (Fig. 2b, d). We next performed *abcc4* knockdown and rescue experiments to verify that *abcc4* was indeed the gene affected in *lkt* mutants. Injection of antisense *abcc4* morpholinos (*abcc4*-MO) caused ciliogenesis defects and phenocopied *lkt* mutants (Supplementary Fig. 3a–h). *abcc4* mRNA injection also rescued *lkt* mutant phenotypes (Supplementary Fig. 4a–i). Together, these findings lead us to conclude that the *lkt* locus encodes ABCC4 and that lkt^{T804M} is a loss of function allele.

Lkt/ABCC4 controls cilia-driven fluid flow in the Kupffer's vesicle

To assess roles of *lkt/abcc4* in ciliogenesis, we examined its expression during embryo development. *lkt/abcc4* transcripts are maternally deposited in cleavage-stage embryos (Fig. 3a), then distributed throughout blastula embryos (Fig. 3b). During somitogenesis, *lkt*/*abcc4* is expressed in neural crest cells, the notochord and KV (Fig. 3c, d). At 36–48 hpf, *lkt*/*abcc4* transcripts are enriched in some of ciliated tissues, including olfactory placodes, otic vesicles, midbrain-hindbrain boundary area and the hindbrain (Fig. 3e–g). Furthermore, *lkt/abcc4* expression coincides with *insulin* expression in the pancreas but not with *wt1b* in the kidney primordium (Supplementary Fig. 3i–n). This may explain why *lkt* mutants do not form kidney cysts (Fig. 1t, u).

Organ laterality in zebrafish is established by cilia-driven fluid flow in KV[19, 20]. Since *lkt/abcc4* deficiency causes a loss of KV cilia (Fig. 1n, o, r, s; Supplementary Fig. 3c), we assessed the status of KV fluid flow in *lkt/abcc4*-deficient embryos. Fluorescent beads were injected into KV of *lkt* mutants and *abcc4* morphants. While both wild-type and control embryos displayed strong directional flow in KV (Fig. 3h, j, p; Supplementary table 1, Supplementary video 1), *lkt* mutants or *abcc4* morphants exhibited absent or reduced KV flow (Fig. 3i, k, p; Supplementary table 1; Supplementary video 2). Given that *lkt/abcc4* is expressed in KV, we evaluated whether *lkt* regulates Nodal signaling autonomously in KV cells by depleting *lkt/abcc4* expression in dorsal forerunner cells (DFCs), precursors of KV cells[21]. Thus, *abcc4*-MO was co-injected with standard fluorescein-MO into the yolk cell at the 1000-cell stage, when yolk-DFC bridges are open, allowing *abcc4*-MO diffusion into DFCs but not into other embryonic cells. The resulting $DFC^{abcc4\text{-}MO}$ mosaic embryos showed random *spaw* expression (Fig. 3n, q). In comparison, normally asymmetric expression of *spaw* was observed in uninjected wild-type embryos, as well as in embryos injected with control-MO ($DFC^{ctrl\text{-}MO}$ embryos), or embryos injected with *abcc4*-MO when yolk-DFC bridges have closed, restricting the morpholinos to the yolk cell ($Yolk^{abcc4\text{-}MO}$) (Fig. 3l, m, o, q). These findings indicate that Lkt/ABCC4 functions autonomously in DFC/KV cells to regulate ciliogenesis and organ laterality.

Lkt/ABCC4 transporter regulates ciliogenesis through PGE2 secretion

Mammalian ABCC4 has been shown to transport several physiological substrates such as prostaglandins, cyclic nucleotides, steroid conjugates and folates [15]. Among related ABCC subfamily members, only ABCC4 is known to directly transport PGE_2[22]. We hypothesized that defective ciliogenesis in *lkt/abcc4* mutants could be caused by diminished PGE_2 export resulting in PGE_2 signaling defects. To test this idea, we assessed whether addition of exogenous PGE_2 could rescue cilia-associated phenotypes in *lkt* mutants. Mutant embryos were incubated in media supplemented with PGE_2 or PGF2α. *lkt* mutants treated with PGE_2 exhibited straight body axis, normal heart looping and otolith biogenesis (Fig. 4a, b; Supplementary Fig. 5a), while all mutants treated with PGF2α showed cilia-associated phenotypes (Supplementary Fig. 5a). We then assessed whether PGE_2 treatment could reverse defective ciliogenesis in *lkt* mutants. In PGE_2-treated *lkt* mutants, reduction of KV cilia number and length was partially reversed (Fig. 4c, d, i, j); restoration of kinocilia or spinal canal cilia was also evident (Fig. 4e–h). Together, these findings are consistent with

the idea that PGE_2 deficiency is responsible, at least in part, for ciliogenesis defects in *lkt* mutants.

To assess whether Lkt/ABCC4 exports PGE_2, we performed PGE_2 efflux assays using *abcc4*-deficient murine embryonic fibroblasts ($MEF^{abcc4-/-}$)[23] expressing human ABCC4, zebrafish Lkt/ABCC4 or mutant Lkt/$ABCC4^{T804M}$. Transfection of human or zebrafish ABCC4 increased extracellular PGE_2 and reduced intracellular PGE_2, relative to vehicle-transfected cells (Fig. 4k). In contrast, cells expressing the Lkt/$ABCC4^{T804M}$ mutant were defective in PGE_2 export (Fig. 4k). Addition of MK571, an inhibitor of ABCC4 transporter[15, 22], blocked ABCC4-mediated PGE_2 export, mimicking the effect of the Lkt/$ABCC4^{T804M}$ mutation (Fig. 4k). These data reveal the molecular bases of Lkt/ABCC4 function, linking PGE_2 export to ciliogenesis. To determine whether zfABCC4 directly exports PGE_2 across the plasma membrane, we performed vesicular transport assays using inside-out membrane vesicles[22, 24]. The ATP-dependent PGE_2 uptake levels were 3-fold greater in vesicles expressing ABCC4 than vesicles derived from untransfected controls (Fig. 4l). We next assessed the sub-cellular localization of mammalian ABCC4 and zebrafish Lkt/ABCC4. Although ABCC4 was reported to localize to the plasma cell membrane, its sub-cellular localization in ciliated cells was not examined[15]. We observed that murine ABCC4 localizes to the plasma cell membrane but not to the cilium in inner medullary collecting duct 3 (IMCD3), ciliated cells (Fig. 4m–o). We next transfected IMCD3 cells with constructs encoding zebrafish *lkt/abcc4* or *lkt/*$abcc4^{T804M}$ mutant gene fused with *EGFP*. Similar to its mammalian counterpart, zebrafish Lkt/ABCC4 protein (EGFP-zfABCC4) was detected on the plasma cell membrane but not in the cilium (Fig. 4p–r). In contrast, Lkt/$ABCC4^{T804M}$ mutant protein (EGFP-zf$ABCC4^{T804M}$) was mis-localized in the cytoplasm in ciliated cells (Fig. 4s–u). Collectively, these findings demonstrate that zebrafish Lkt/ABCC4 has a strong activity in exporting PGE_2, whereas the T804M mutation, likely due to its loss of normal membrane localization, is incapable of PGE_2 export.

COX-EP4 signaling regulates Lkt/ABCC4-mediated ciliogenesis

PGE_2 is synthesized by COX-1 and COX-2, and after secretion from the cell, it binds and signals through G-protein-coupled receptors EP1–4[1, 3]. Knowing that *cox1*, *cox2* and *ep4* are expressed during zebrafish development[25–28], where *cox1* is expressed in the gastrula and *cox2* is detected in the anterior neuroectoderm[25], we assessed whether embryos deficient in PGE_2 signaling exhibit ciliogenesis defects. Microinjection of *cox1*-MO[25, 27] into wild-type embryos at low doses caused cilia-associated phenotypes, including hydrocephalus, randomized heart looping, abnormal otolith number and curved body axis (Fig. 5a–c, g–h; Supplementary Fig. 5h, i), whereas *cox2*-MO[25, 27] injection resulted in hydrocephalus, abnormal otoliths and curved body axis, but did not affect heart looping (Fig. 5g, h; Supplementary Fig. 5b, c; h, i). DFC/KV-targeted injection of *cox1*-MO but not *cox2-MO* caused a decrease in KV cilia number and length (Fig. 5i, j; u, v). These findings are consistent with the expression patterns of *cox1* and *cox2* during zebrafish development[25]. Embryos injected with both *cox1*-MO and *cox2*-MO displayed even more severe cilia-related abnormalities (Fig. 5g; Supplementary Fig. 5h, i). $lkt^{+/-}$ heterozygous embryos and wild-type homozygous embryos injected with *cox1*-MO or *ep4*-MO display comparable

percentages of cilia-associated phenotypes (Supplementary Fig. 6a, b), indicating that a partial loss of *lkt/abcc4* function does not sensitize the embryo to the reduction of PGE_2 signaling. Finally, microinjections of either *cox1*-MO or *cox2*-MO at low doses caused cilia loss in ears and the spinal canal (Fig. 5o–q; Supplementary Fig. 5d, e, f). These cilia defects and malformations are partially rescued by the PGE_2 addition (Fig. 5k, r, g, h, u, v; Supplementary Fig. 5h, i). Thus, PGE_2 synthesis is required for normal ciliary development.

To evaluate whether EP4 acts as a receptor of Lkt/ABCC4-mediated PGE_2 signaling during ciliogenesis, we performed EP4 knockdown experiments. Injection of *ep4*-MO[25, 27] targeting DFC/KV cells caused cilia loss and length reduction in KV (Fig. 5i, l; u, v), whereas injection of *ep4*-MO (1 ng) into one-cell embryos caused loss of kinocilia in ears and the spinal canal (Fig. 5o, s; Supplementary Fig. 5g), resulting in multiple organ defects similar to *lkt* mutants (Fig. 5d–f, g, h; Supplementary Fig. 5h, i). PGE_2 addition failed to reverse cilia loss or organ malformation in *ep4*-deficient embryos (Fig. 5l, m, g, h, u, v; Supplementary Fig. 5h, i), indicating that EP4 acts downstream of secreted PGE_2 required for ciliogenesis. Furthermore, co-injection of *cox1* mRNA, *cox2* mRNA and *ep4* mRNA with *cox1*-MO, *cox2*-MO and *ep4*-MO, respectively, suppressed hydrocephalus, indicating the functional specificity of *cox1*-MO, *cox2*-MO and *ep4*-MO (Supplementary Fig. 4j). EP4 is a GPCR that activates Gs to increase the intracellular cAMP[3], which, in turn, activates PKA and promote ciliogenesis[29]. Addition of forskolin (FSK), an activator of adenylate cyclase, suppressed partially cilia loss in KV and ears (Fig. 5l, n; s, t; u, v), and reversed organ malformation in *ep4*-morphants (Fig. 5g, h; Supplementary Fig. 5h, i). The expression of transcription factors Foxj1a and Foxj1b, which are required for cilia biosynthesis[30, 31], is not altered in *lkt* mutants, *cox1/cox2* morphants or *ep4* morphants (Supplementary Fig. 6c–n), suggesting that COX-Lkt/ABCC4-EP4 signaling functions downstream or in parallel to their function by activating cAMP signaling in promoting ciliogenesis.

We next assessed roles of PGE_2 signaling in ciliogenesis using pharmacological approaches. Administration of wild-type embryos with SC560 (Cox1 inhibitor), AH23848 (Ep4 inhibitor) or indomethacin (Cox1 and Cox2 inhibitor) at relevant time frames resulted in cilia-associated phenotypes (Fig. 6a–d) and cilia defects in ears and KV (Fig. 6e–g; h–i), similar to these seen in embryos injected with *cox1*-MO, *ep4*-MO, or both *cox1*-MO and *cox2*-MO. In contrast to that, administration of Cox2 inhibitor NS398 only caused hydrocephalus and three otoliths but not randomized heart laterality and KV cilia reduction (Fig. 6a–d; h, i), thus phenocopying *cox-2* morphants. Moreover, Indomethacin treatment in *lkt* mutants exacerbated ciliogenesis defects in KV and ears (Fig. 6j–q). These findings complement our antisense knockdown studies and refine our understanding of time frames when PGE_2 singling functions in ciliogenesis.

Lkt/ABCC4 function in ciliogenesis is conserved in mammalian cells

To assess roles of Lkt/ABCC4-mediated PGE_2 signaling in ciliogenesis in mammalian cells, we depleted ABCC4 or EP4 in human retinal pigment epithelial 1 (hRPE1) cells using short-interfering RNA (siRNA)[32]. Immunoblotting confirmed that both ABCC4 and EP4 protein levels were significantly reduced in cells transfected with ABCC4-siRNA or EP4-siRNA (Fig. 7e, f). We observed that depletion of ABCC4 or EP4 in hRPE1 cells caused a reduction

of ciliaformation and elongation when compared with use of the control siRNA (Fig. 7a, b, c). Bothcilia length and percentages of ciliated cells were significantly reduced in ABCC4 or EP4 depleted cells (Fig. 7g. h). Addition of exogenous PGE_2 increased both cilia length and percentages of ciliated cells in control cells but not in EP4-depleted cells (Fig. 7a, d; g, h), indicating that EP4 acts downstream of PGE_2 signaling during ciliogenesis. Moreover, depletion of ABCC4 or EP4 in IMCD3 cells resulted in similar results to those in hRPE1 cells (Supplementary Fig. 8a–h). We next assessed the sub-cellular localization of human EP4. EP4 staining in the plasma cell membrane has been described previously[33]. We observed that EP4 localizes to the cilium and is enriched in the perciliary cell membranę in hRPE1 cells (Fig. 7i–k). Similar ciliary localization of EP4 was also seen in IMCD3 cells (Fig. 7l). Consistent with the plasma membrane localization of murine and zebrafish Lkt/ABCC4 transporters (Fig. 4m–r), human ABCC4 also localizes to the plasma membrane but not to the cilium (Fig. 7m, n), whereas EP4 is detected on the cilum in the same hRPE cell (Fig. 7m, n). Collectively, these findings suggest that PGE_2 released by ABCC4 binds and signals through the EP4 receptor in the cilium.

PGE_2 signaling affects anterograde velocity of IFT during ciliogenesis

cAMP signaling is known to promote ciliogenesis by increasing anterograde IFT[29]. Given that PGE_2 acts upstream of cAMP signaling, we assessed the possibility that Lkt/ABCC4-mediated PGE_2 signaling regulates ciliogenesis via the control of IFT. To test this idea, we imaged the movement of IFT particles in IMCD3 cells stably expressing IFT88-EYFP using time-lapse microscopy[34]. As expected, we observed that IFT particles are transported along axonemal microtubules from the ciliary base to the tip of the cilium (Fig. 8a). To determine velocities of individual IFT88 particles, the time-lapse image sequences were converted into kymographs (Fig. 8b–d). We observed that similar to FSK treatment[29], PGE_2 increased anterograde velocities of IFT88 particles but had no obvious effects on retrograde velocities (Fig. 8g; Supplementary Fig. 7). Moreover, PGE_2-treated cells displayed more intense fluorescence at the cilium tip revealing accumulation of IFT88 particles (Fig. 8e, f). Furthermore, we found that PGE_2 treatment partially rescues cilia defect in *oval*/*ift88* mutants (Fig. 8h, i, l, n). A rescue is not observed however for *elipsa*/*ift54* at this stage (Fig. 8j, k, m, n). This is most likely due to the fact that *elipsa/ift54* phenotype is more severe, compared to that seen in *oval/ift88*[7, 35]. These observations are consistent with the increased IFT velocity and efficiency in PGE_2-treated cells. Hence, PGE_2 signaling increases the anterograde speed of IFT, thereby accelerating the movement of cargos into the axoneme and resulting in enhanced ciliogenesis.

DISCUSSION

In this study, we demonstrate that normal cilia formation and elongation require the COX-Lkt/ABCC4-EP4 signaling cascade. While ABCC4 has the ability to transport a variety of physiological metabolites[15], the current study reveals a crucial and unexpected role for Lkt/ABCC4-mediated PGE_2 export in ciliogenesis. cAMP-dependent kinase signaling is known to increase anterograde IFT during ciliogenesis[29]. Our data suggest that Lkt/ABCC4-mediated PGE_2 signaling affects cAMP level and promotes ciliogenesis via an increase in the anterograde velocity of IFT. These results reveal a conserved ciliogenic cascade. A

model is proposed where PGE_2 is exported from cells via Lkt/ABCC4 on the plasma cell membrane and signals through the EP4 receptor on the cilium or at the base of the cilium, thereby activating Gs and cAMP signaling to promote the anterograde IFT (Fig. 8o). In support of this model, we found that PGE_2 treatment causes an increase of intracellular cAMP but not Ca^{2+} during ciliogenesis in IMCD3 cells (Supplementary Fig. 8i, j), which is consistent with PGE_2 studies in other cells and tissues[36, 37]. Furthermore, adenylate cyclase is detected in the cilium[38]. Cilia formation requires coordinated regulation of the bidirectional IFT particle traffic, including its frequency and speed[39, 40]. The dynamic modulation of IFT velocity by COX-Lkt/ABCC4-EP4 signaling represents a key regulatory step in axoneme formation and elongation. PGE_2 is derived from the prostaglandin precursor, PGH_2, which is biosynthesized by COX1 and COX2 enzymes from arachidonic acid, a 20-carbon polyunsaturated fatty acid[1, 41]. We propose that after being exported from cells, PGE_2 acts in an autocrine and/or paracrine manner, as it is known that cells can respond to PGE_2 released by either themselves or by their neighbors[42].

In human cancer cells, interaction of PGE_2 with EP4 receptor induces Wnt/β-catenin signaling resulting in COX2 expression, thereby setting up a positive feedback loop leading to further PGE_2 synthesis[42]. Such positive feedback loop in PGE_2 autocrine signaling mechanism may enable cells in the epithelial field of the KV or the otic vesicle to rapidly upregulate ciliogenesis[43]. This effect may be further enhanced by paracrine PGE_2 signaling between neighboring cells. The interplay between PGE_2 autocrine and paracrine signaling may create a community effect, whereby all cells in the epithelial field are coherently activated to generate cilia and ciliary motility. Although PGE_2 is implicated in influencing the ciliary beat frequency of cultured nasal mucosa cells[44], the role of PGE_2 signaling in cilia formation was not reported in previous murine genetic studies[45–47]. This is most likely due to the presence of maternal contribution of prostaglandins in the placenta, which allows PGE_2-deficient mouse embryos to develop normally[48]. The use of externally developing zebrafish embryos allowed us to reveal the ciliogenenic roles of PGE_2 signaling. In agreement with animal model studies, cultured mammalian cells deficient in PGE_2 signaling also display defective ciliogenesis. Given the role of cilia dysfunction in human disorders[49, 50], our findings suggest the existence of a previously unexplored aspect of human ciliopathies arising from abnormal prostagladin signaling.

Methods

Zebrafish maintenance

Zebrafish (Danio rerio, AB line) care and breeding were described previously[1]. Embryos were staged according to their morphology[51]. *lkt* mutants were isolated from a large-scale N-ethyl-N-nitrosourea (ENU) mutagenesis (Boston screen 2000)[52]. Fudan Animal Care Committee advises animal care and research.

Genetic mapping and positional cloning of *lkt*

Genetic mapping, whole genome bulk segregant analyses and positional cloning of *lkt* were conducted as previously described[14]. The genomic region covering the *lkt* interval was defined by genotyping 1745 mutant embryos (3490 meioses) using single strand length

polymorphism (SSLP) markers Z17212 and Z6907. Additional SSLP markers VU1 (F: 5′-CAATGCCAATCAGCTCCATA; R: 5′-AGCAACGACGCTACCAAAAA) and VU2 (F: 5′-GGGTGAGGAGGCTTTTTGTC; R: 5′-AGATGATTGCTTCCAGCACA) were generated using genomic sequence (http://www.ensembl.org/Danio_rerio/index.html) between Z17212 and Z6907. BAC241A1 was identified in the sequence contig flanked by Z17212 and Z6907. Several single nucleotide polymorphism (SNP) markers were generated by sequencing intron regions and 3′-UTR in *abcc4*, including SNP1 (F: 5′-TAGCCTGGAAGTGCCTGATGT; R: 5′-ATGAGAATTAGTTGGCATGTAG) and SNP2 (F: 5′-GTGTTTGTGGTATTCTGAAGG; R: 5′-AGTCCGGACTGCTGAAGCTC). Total RNAs were extracted using Trizol (Invitrogen) from wild-type (Wt) and *lkt* mutant embryos. Eight independent clones from mutant and Wt embryos were subjected to sequencing analyses. A 4.5 kb PCR product of *lkt* from Wt embryos was amplified using primers abcc-Sac and abcc-Eco (abcc-Sac: 5′-ACTGCCGCGGATGGAGCCGATAAAGAAAGATGC; abcc-Eco: 5′-ACTGGATATCAACGGTCTTAATTGCTG) and subcloned into expression vector pcGlobinII by EcoRV/SacII. Four base changes were detected between Wt and *lkt* mutants. Through sequencing the genomic regions in multiple Wt strains, including EK, TL and AB, and *lkt* mutants, three of these changes (S691L, V719L and T1301A) were determined to be polymorphisms, and one change at amino acid 804 from ACG to ATG was determined to be a genuine *lkt* mutation.

In situ hybridization and immunofluorescence analysis

Single label whole-mount in situ hybridization and immunofluorescent staining were described previously[53]. To generate *lkt/abcc4* (GenBank: EU586042.1) in situ probes, a 1.8 kb *lkt* fragment was amplified from pcGlobin-lkt plasmid by primers abcc-F5 and abcc-Eco (abcc-F5: 5′-TTCATTCAGGTGTTTCTGCA; abcc-Eco: 5′-ACTGGATATCAACGGTCTTA ATTGCTG) and subcloned into pCRII-TOPO vector (Invitrogen). *lkt* antisense probes were synthesized with SP6 RNA polymerase (Roche) using HindIII linearized pCRII-TOPO-lkt constructs. Double in situ hybridization was conducted as described[54]. The embryos were hybridized simultaneously with digoxigenin-labeled *lkt/abcc4* antisense probes and fluorescein-labeled *insulin* or *wt1b* antisense probes, then incubated with anti-digoxigenin conjugated to alkaline phosphatase Fab fragments (Roche) and detected by NBT/BCIP (Roche). To inactivate anti-digoxigenin alkaline phosphatase antibodies, embryos were fixed in 4% paraformaldehyde and incubated in 10 mM EDTA in MABT (maleic acid buffer containing Tween 20) for 10 minutes at 70°C. Following rehydration, embryos were incubated with anti-fluorescent alkaline phosphatase Fab fragments (Roche) and were visualized with INT/BCIP (Roche). Cilia immunofluorescence in KV, ears, spinal cord or otic vesicles was performed using anti-acetylated tubulin monoclonal antibody[20] (1:200; Sigma, T6793). KV cilia were visualized by double immunofluorescence using anti-acetylated tubulin antibody, anti-αPKC rabbit antibody[9] (1:100; Santa Cruz Biotechnology, sc-216). Secondary antibodies include Alexa Fluor 555 goat anti-mouse IgG (H+L) (1:1000; Life Technologies, A21434) and Alexa Fluor 488 goat anti-rabbit IgG (H+L) (1:1000; Life Technologies, A11008). Stained embryos were mounted in 1% low melting agarose and imaged using a 63×water-dipping objective on a Zeiss LSM710 Laser Scanning Confocal Microscope.

Antisense morpholinos, mRNAs design and injection

Antisense morpholinos were designed and synthesized by Gene Tools, LLC. *lkt*/*abcc4*-MO (5′-CATTAGGACTGACCTTTCCAGCTCC) targets the donor site of intron10. Control morpholinos (Ctrl-*lkt/abcc4*-MO) contains 5 mismatched nucleotides, which are underlined in *lkt*/*abcc4*-MO (5′-CATTACGACTGAGCATAGCAGCTCC). *cox1*-MO (5′-TCAGCAAAAAGTTACACTCTCTCAT), *cox2*-MO (5′-GCTGTTGAAGCAGAGATGCGTTACT) and *ep4*-MO (5′–CACGGTGGGCTCCATGCTGCTGCTG) were designed as previously described (ref.25, 27). MO injections were conducted as described to generate whole embryo knockdowns[3] or DFC^{MO} mosaic embryos[21]. Standard fluorescein-tagged morpholinos (fluorescein-MO) (ref. 21) were used to create $DFC^{ctrl\text{-}MO}$. For generating DFC^{MO} mosaic embryos, *lkt/abcc4*-MO, *ep4*-MO or both *cox1*-MO and *cox2*-MO were co-injected with standard fluorescein-tagged morpholinos (fluorescein-MO) into the yolk cell at ~1000-cell stage. Embryos, in which fluorescein-MO diffused throughout the yolk and entered the DFC/KV cells but not other embryoic cells, were selected for mosiac analyses. For $DFC^{ctrl\text{-}MO}$ embryos, fluorescein-MO were injected into the yolk cell at ~1000-cell stage. For $yolk^{lkt\text{-}MO}$ embryos, *lkt*-MO was injected with fluorescein-MO into the yolk cell between the dome stage and 30% epiboly stage, when connections between the yolk and DFC precursors have closed and morpholinos are restricted to the yolk cell. For rescue experiments, whole-length capped mRNAs of *abcc4*, *cox1*, *cox2* and *ep4* were synthesized using mMessage mMachine SP6 kit (Ambion, AM1340). Since *cox1*-MO inhibits the ATG start codon, *cox1* mRNA was designed to contain 5 mismatched nucleotides (underlined: 5′-ATGAGGGAAT CAATTTCTTG CTGA) so that it could not be bound by the *cox1*-MO in rescue experiments involving injection of mRNA and morpholino at the same time. As *ep4*-MO, *cox2*-MO and *abcc4*-MO were designed against 5′-UTR and splicing sties, wild-type mRNAs of *abcc4*-MO, *cox2*-MO and *ep4*-MO were synthesized.

Drug treatments

PGE_2 (Sigma, P0409), $PGF_2\alpha$ (Santa Cruz Biotechnology, SC-201227), SC560 (Sigma, S2064), AH23848 (Sigma, A8227) were dissolved in DMSO for a 50 mM stock solution. NS398 (Cayman, 70590) and Indomethacin (Sigma, I7378) were dissolved in DMSO to a 100 mM stock solution. Embryos were incubated in embryo media containing drugs at desired concentrations at relevant timeframes (see Figure 6 Legends), and then subjected to phenotype and immunostaining analyses.

Video microscopy analysis of KV fluid flow and cilia motility

Fluorescent beads (Polysciences, Inc.) were injected into KV and fluid flow was analyzed as previously described[19]. Details of videomicroscopy analysis of KV flow and cilia motility were described[19]. Flow was imaged using a Zeiss Axio Imager M1 microscope with a 63x Plan Apochromat water-dipping objective. Movies were generated using a Zeiss Axiocam high speed monochromatic digital camera and Axiovision (Zeiss) and Quicktime (Apple) software.

PGE2 cell export assay

Extracellular and intracellular PGE_2 were extracted and measured using PGE_2 EIA kit (Enzo Life sciences). $MEF^{abcc4-/-}$ Cells transfected with pAcGFP-huABCC4, pAcGFP-zfABCC4 or pAcGFP-zfABCC^{T804M} were seeded into six-well plates at 2×10^5 cells/well in 1 ml of complete medium. 24hr after the transfection 1ml fresh DMEM 10% FBS media was fed to the transiently transfected cells. Supernatant was collected and processed for measurement of extracellular PGE_2 levels after 12h incubation. Purification of extracellular PGE_2 was accomplished using C-18 mini columns. Cell monolayer was rinsed twice with ice-cold PBS and cells were collected by scraping into 1 ml of ice-cold PBS. Cells were pelleted and stored at 80°C before the purification of intracellular PGE_2. Frozen cell pellets were taken up in 1 ml of homogenization buffer and then sonicated briefly three times in 3-second bursts. Duplicate sets of samples were saved for determination of cellular protein concentrations using western analysis. An aliquot of each sample was spiked with PGE_2 (20 pg) before purification for monitoring the recovery rate. After the addition of 1 ml of acetone, samples were vortexed, allowed to stand for 20 min and centrifuged at 25°C for 10 min; the acetone was then evaporated under a gentle stream of nitrogen. The pH of samples was adjusted to 4.0 using 1N HCl and the C-18 columns were activated before addition of sample with 10 ml of ethanol and 10 ml of water. After the sample addition, columns were washed with 10 ml of 15% ethanol followed by 10 ml of hexanes and PGE_2 was eluted with 10 ml of ethyl acetate. Samples were subsequently dried under a gentle stream of nitrogen for the ELISA PGE_2 determinations.

PGE2 vesicular transport assay

Membrane vesicles were prepared from both the SV40-transformed HEK293T cells and those cells transiently expressing pAcGFP-zfABCC4. pAcGFP-zfABCC4 was transfected into HEK293T cells using PolyJet (FroggaBio) after 48 h, inside-out membrane vesicles were prepared and zfAbcc4 levels in the membrane vesicles were confirmed by immunoblotting using Living Colors® EGFP(Clonetech). ATP-dependent uptake of ^{3}H-labeled prostaglandin E_2 (PGE_2) (180 Ci/mmol) by the membrane vesicles was measured using a rapid filtration technique. Briefly, 30 μl reaction mixtures containing 5 μM [^{3}H]PGE_2 (100 nCi), 4 mM AMP or ATP, 10 mM $MgCl_2$, and membrane vesicle protein (10 μg) were incubated at 37°C for 10 min. Uptake was stopped by rapid dilution of the reaction mixtures in ice-cold buffer and vesicles were immediately collected by filtration through a Unifilter-96 GF/B plate (Perkin Elmer) using a Packard Filtermate harvester. Tritium associated with the vesicles was counted using a Top Count NXT microplate scintillation counter (Perkin Elmer). Uptake in the presence of AMP was subtracted from uptake in the absence of ATP to determine ATP-dependent uptake values. Experiments were carried out in duplicate and repeated twice.

Cell culture, siRNA and immunostaining analyses

Primary IMCD3 (ATCC®CRL-2123™)[32] and hRPE1 cells (ATCC® CRL-4000™)[32] were plated on Poly-L-Lysine-coated cell culture plates and were cultured at 37°C, 5% CO_2 in DMEM/F12 medium (GIBCO) containing 10% FBS. At 60% confluence, IMCD3 cells were transfected with ABCC4 siRNA at 75 nM (Qiagen; SIO2833040, 5′–

AAGGACCTTGTGATTAG TCAA; SIO2833019, 5′–AACGGATGAGTTAATACAACA), EP4 SMARTpool siRNA at 100 nM (Dharmacon; M-048700-01-0005; 5′–CTAGAGAACAGGCGAGCTC, 5′–CAGCTAATATTGTC GATGT, 5′–CCACCAACGTAACGGCCTA, 5′–CCAGTGAAACTCTGAAATT) or control siRNA (Ribo; siN-05815122147) at 100 nM using Lipofectamine RNAimax (Life Technologies). hRPE1 cells were transfected with 100 nM ABCC4 siRNA (Ribo; siG-000010257A; 5′–GAGCAATCATAAAGTGTTA), 100 nM EP4 SMARTpool siRNA (Dharmacon; M-005714-00-0005; 5′–CTGAGGACTTTGCGAATAT, 5′–GTGAAACACTGAACTTATC, 5′–CATCAACCATGCCTATTTC, 5′–TATATATCCTCCTGAGAAA) or 100 nM control siRNA using Lipofectamine RNAimax (Life Technologies). To examine cilia formation, the culture medium was switched to DMEM containing 0.5% FBS for 48 h after transfection and incubation for 24 h. Both IMCD3 and hRPE1 cells were then treated with 100 μM Forskolin (Sigma, F6886), 10 μM PGE2 (Sigma) or 0.1% DMSO (Control) for 12 hours. Treated cells were fixed in 4% PFA at room temperature for 20 minutes, permeabilized in 0.2% Triton X-100 in PBS for 20 minutes, and blocked in 2% heat-inactivated goat serum for 60 minutes prior to staining with antibodies against acetylated -tubulin[26] (1:1000; Sigma, T6557), ARL13B (1:1000; Proteintech, 17711-1-AP) and DAPI (Invitrogen). To determine the sub-cellular location of EP4 and ABCC4 proteins in cilia cells, antibodies against EP4 (1:100; Santa Cruz Biotechnology, sc-55596)[55, 56], ABCC4 (1:50; Alexis Biochemical, ALX-801-038-C150)[57, 58] and antibodies against EGFP (1:1000; Abcam, ab5450) were used. Secondary antibodies used include Alexa Fluor 488 goat against mouse IgG (H+L) (1:1000; Life Technologies, A11001), Alexa Fluor 555 goat against rat IgG (H+L) (1:1000; Life Technologies, A21434), Alexa Fluor 594 goat against mouse IgG (H+L) (1:1000; Life Technologies, A11005), Alexa Fluor 594 goat against rabbit IgG (H+L) (1:1000; Life Technologies, A11012) and Alexa Fluor 488 donkey against goat IgG (H+L) (1:1000; Life Technologies, A11055). Imaging was performed using a Zeiss Axio Observer inverted fluorescence Imaging was performed using Zeiss Axio Observer inverted fluorescence microscope with a 63x NA1.15 water-dipping objective.

Live cell imaging of intraflagellar transport

M368-4 cells (clonal line of IMCD3 cells stably expressing IFT88-EYFP, a gift from Jagesh V. Shah, Harvard Medical School, Boston, USA; ref. 34) were cultured and treated with 10 μM PGE2 (Sigma) for 12 hours and DMSO, respectively. Cells were plated on Poly-L-Lysine-coated glass coverslips and were cultured at 37°C, 5% CO_2 in DMEM medium containing 10% FBS until reaching 100% confluency. Cells were examined for IFT88 movement at 37°C on an OLYMPUS ZX81 inverted microscope system equipped with a spinning disk confocal head (ANDOR) using a 150 x oil immersion objective (1.45 NA). Time-lapse images (200 frames) were captured continuously with exposure 150 ms and 7 frames per second. Time-lapse image sequences were assembled into kymographs and the velocities of IFT88-EYFP particles was calculated using the ImageJ software package (http://rsbweb.nih.gov/ij) as described (ref. 29, 34).

Cyclic AMP measurement

IMCD3 cells were cultured in DMEM containing 10% fetal bovine serum, 5% CO2, 1% penicillin and streptomycin at 37°C. IMCD3 cells were treated with 100 μM Forskolin (Sigma), 10 μM PGE2 (Sigma) or DMSO (vehicle only) for 3 hours. Treated IMCD3 were lysed in 0.1M HCl, and then centrifuged to pellet cellular debris. Supernatants were aspirated to measure cAMP concentrations using complete ELISA kit (ENZO, Life Science, ADI-901-163).

Calcium measurement

IMCD3 cells were cultured in DMEM containing 10% fetal bovine serum, 1% penicillin and streptomycin, 5% CO2, at 37°C overnight. IMCD3 cells were treated with 100 μM Forskolin (Sigma), 10 μM PGE2 (Sigma) or DMSO (vehicle only) for 3 hours and then incubated with 5 μM Fura-2-acetoxymethyl ester (Sigma, 47989) for 1 hour at 37°C. Calcium concentrations were measured using an inverted fluorescent microscope (Nikon Eclipse Ti). Calcium concentration was indicated as the ratio of fluorescence intensity at excitation wavelengths of 340 and 380 nm (F ratio).

Statistics Methods

For comparing two independent groups on a given variable, independent sample t-tests are justified when the dependent variable is normally distributed. When the normality assumption is violated, non-parametric Mann-Whitney U Tests are justified to be appropriate. For determining independent association between two categorical variables, non-parametric Chi-square tests are justified. For Student t-test, the minimal sample size for embryo was determined to be 10 and the minimal sample size for cell was determined to be 50. This sample size is able to detect a standardized effect size 0.2 and to reject the null hypothesis that the two population means are equal with probability (power) 0.85. For continuity-corrected chi-square test, the minimal sample size for embryo was determined to be 20. This gives power 0.80 to detect true difference 0.4 with default Type I error probability 0.05. Each subject (embryo, cell or image field) was randomly chosen and allocated to their respective group, and we were not blinded to the group allocation.

Supplementary Material

Refer to Web version on PubMed Central for supplementary material.

Acknowledgments

We acknowledge Peng Yuanyuan and John Guan for invaluable assistance in fish care, Xueliang Zhu for hRPE1 cells, Jagesh Shah for IFT88-EYFP cells, Chen Yi for cAMP assays, Qiao Li for diagram drawing, Liang Cai and Genfeng Zhu for spin-disk confocal microscopy analysis. We are grateful to Hong Ma, Bruce Appel, Zhaoxia Sun, Joshua Gamse and members of our laboratories for comments on the manuscript and helpful discussions. This research was supported in part by grants from National Basic Research Program of China (CMST2013CB945301, CMST2012CB944501; TPZ), National Natural Science Foundation of China (NSFC31172173; TPZ), Shanghai Pujiang Program (11PJ1401600; TPZ) as well as National Institute of Health of America (TPZ, JDS, JM, IAD) and Canadian Institutes of Health Research (MOP106513, SPCC).

References

1. Smith WL, DeWitt DL, Garavito RM. Cyclooxygenases: structural, cellular, and molecular biology. Annu Rev Biochem. 2000; 69:145–182. [PubMed: 10966456]
2. Langenbach R, Loftin CD, Lee C, Tiano H. Cyclooxygenase-deficient mice. A summary of their characteristics and susceptibilities to inflammation and carcinogenesis. Ann N Y Acad Sci. 1999; 889:52–61. [PubMed: 10668482]
3. Narumiya S, Sugimoto Y, Ushikubi F. Prostanoid receptors: structures, properties, and functions. Physiol Rev. 1999; 79:1193–1226. [PubMed: 10508233]
4. Goetz SC, Anderson KV. The primary cilium: a signalling centre during vertebrate development. Nat Rev Genet. 2010; 11:331–344. [PubMed: 20395968]
5. Gerdes JM, Davis EE, Katsanis N. The vertebrate primary cilium in development, homeostasis, and disease. Cell. 2009; 137:32–45. [PubMed: 19345185]
6. Nachury MV, et al. A core complex of BBS proteins cooperates with the GTPase Rab8 to promote ciliary membrane biogenesis. Cell. 2007; 129:1201–1213. [PubMed: 17574030]
7. Omori Y, et al. Elipsa is an early determinant of ciliogenesis that links the IFT particle to membrane-associated small GTPase Rab8. Nat Cell Biol. 2008; 10:437–444. [PubMed: 18364699]
8. Fliegauf M, Benzing T, Omran H. When cilia go bad: cilia defects and ciliopathies. Nat Rev Mol Cell Biol. 2007; 8:880–893. [PubMed: 17955020]
9. Neugebauer JM, Amack JD, Peterson AG, Bisgrove BW, Yost HJ. FGF signalling during embryo development regulates cilia length in diverse epithelia. Nature. 2009; 458:651–654. [PubMed: 19242413]
10. Caron A, Xu X, Lin X. Wnt/beta-catenin signaling directly regulates Foxj1 expression and ciliogenesis in zebrafish Kupffer's vesicle. Development. 2012; 139:514–524. [PubMed: 22190638]
11. Lopes SS, et al. Notch signalling regulates left-right asymmetry through ciliary length control. Development. 2010; 137:3625–3632. [PubMed: 20876649]
12. Sarmah B, Winfrey VP, Olson GE, Appel B, Wente SR. A role for the inositol kinase Ipk1 in ciliary beating and length maintenance. Proc Natl Acad Sci U S A. 2007; 104:19843–19848. [PubMed: 18056639]
13. Long S, Ahmad N, Rebagliati M. The zebrafish nodal-related gene southpaw is required for visceral and diencephalic left-right asymmetry. Development. 2003; 130:2303–2316. [PubMed: 12702646]
14. Zhong TP, Rosenberg M, Mohideen MA, Weinstein B, Fishman MC. gridlock, an HLH gene required for assembly of the aorta in zebrafish. Science. 2000; 287:1820–1824. [PubMed: 10710309]
15. Russel FG, KJB, Masereeuw R. Multidrug resistance protein 4 (MRP4/ABCC4): a versatile efflux transporter for drugs and signalling molecules. Trends Pharmacol Sci. 2008; 29:200–207. [PubMed: 18353444]
16. Schuetz JD, et al. MRP4: A previously unidentified factor in resistance to nucleoside-based antiviral drugs. Nat Med. 1999; 5:1048–1051. [PubMed: 10470083]
17. Slot AJ, Molinski SV, Cole SP. Mammalian multidrug-resistance proteins (MRPs). Essays Biochem. 2011; 50:179–207. [PubMed: 21967058]
18. Schuldiner S. The ins and outs of drug transport. Nature. 2006; 144:156–157. [PubMed: 16971936]
19. Essner JJ, Amack JD, Nyholm MK, Harris EB, Yost HJ. Kupffer's vesicle is a ciliated organ of asymmetry in the zebrafish embryo that initiates left-right development of the brain, heart and gut. Development. 2005; 132:1247–1260. [PubMed: 15716348]
20. Kramer-Zucker AG, et al. Cilia-driven fluid flow in the zebrafish pronephros, brain and Kupffer's vesicle is required for normal organogenesis. Development. 2005; 132:1907–1921. [PubMed: 15790966]
21. Amack JD, Yost HJ. The T box transcription factor no tail in ciliated cells controls zebrafish left-right asymmetry. Curr Biol. 2004; 14:685–690. [PubMed: 15084283]

22. Reid G, et al. The human multidrug resistance protein MRP4 functions as a prostaglandin efflux transporter and is inhibited by nonsteroidal antiinflammatory drugs. Proc Natl Acad Sci U S A. 2003; 100:9244–9249. [PubMed: 12835412]
23. Fukuda Y, et al. Human immunodeficiency virus protease inhibitors interact with ATP binding cassette transporter 4/multidrug resistance protein 4: a basis for unanticipated enhanced cytotoxicity. Mol Pharmacol. 2013; 84:361–371. [PubMed: 23775562]
24. Conseil G, Deeley RG, Cole SP. Functional importance of three basic residues clustered at the cytosolic interface of transmembrane helix 15 in the multidrug and organic anion transporter MRP1 (ABCC1). J Biol Chem. 2006; 281:43–50. [PubMed: 16230346]
25. Cha YI, et al. Cyclooxygenase-1-derived PGE2 promotes cell motility via the G-protein-coupled EP4 receptor during vertebrate gastrulation. Genes Dev. 2006; 20:77–86. [PubMed: 16391234]
26. Cha YI, Kim SH, Solnica-Krezel L, Dubois RN. Cyclooxygenase-1 signaling is required for vascular tube formation during development. Dev Biol. 2005; 282:274–283. [PubMed: 15936346]
27. North TE, et al. Prostaglandin E2 regulates vertebrate haematopoietic stem cell homeostasis. Nature. 2007; 447:1007–1011. [PubMed: 17581586]
28. Goessling W, et al. Genetic interaction of PGE2 and Wnt signaling regulates developmental specification of stem cells and regeneration. Cell. 2009; 136:1136–1147. [PubMed: 19303855]
29. Besschetnova TY, et al. Identification of signaling pathways regulating primary cilium length and flow-mediated adaptation. Curr Biol. 2010; 20:182–187. [PubMed: 20096584]
30. Yu X, Ng CP, Habacher H, Roy S. Foxj1 transcription factors are master regulators of the motile ciliogenic program. Nat Genet. 2008; 40:1445–1453. [PubMed: 19011630]
31. Stubbs JL, Oishi I, Belmonte JCI, Kintner C. The forkhead protein Foxj1 specifies node-like cilia in Xenopus and zebrafish embryos. Nature Genetics. 2008; 40:1454–1460. [PubMed: 19011629]
32. Cao J, et al. miR-129-3p controls cilia assembly by regulating CP110 and actin dynamics. Nat Cell Biol. 2012; 14:697–706. [PubMed: 22684256]
33. St-Jacques B, Ma W. Prostaglandin E2/EP4 signalling facilitates EP4 receptor externalization in primary sensory neurons in vitro and in vivo. Pain. 2013; 154:313–323. [PubMed: 23265688]
34. Tran PV, et al. THM1 negatively modulates mouse sonic hedgehog signal transduction and affects retrograde intraflagellar transport in cilia. Nat Genet. 2008; 40:403–410. [PubMed: 18327258]
35. Tsujikawa M, Malicki J. Intraflagellar transport genes are essential for differentiation and survival of vertebrate sensory neurons. Neuron. 2004; 42:703–716. [PubMed: 15182712]
36. Boyce JA. Mast cells and eicosanoid mediators: a system of reciprocal paracrine and autocrine regulation. Immunol Rev. 2007; 217:168–185. [PubMed: 17498059]
37. Starner RJ, McClelland L, Abdel-Malek Z, Fricke A, Scott G. PGE(2) is a UVR-inducible autocrine factor for human melanocytes that stimulates tyrosinase activation. Exp Dermatol. 2010; 19:682–684. [PubMed: 20500768]
38. Wang Z, Phan T, Storm DR. The type 3 adenylyl cyclase is required for novel object learning and extinction of contextual memory: role of cAMP signaling in primary cilia. J Neurosci. 2011; 31:5557–5561. [PubMed: 21490195]
39. Engel BD, Ludington WB, Marshall WF. Intraflagellar transport particle size scales inversely with flagellar length: revisiting the balance-point length control model. J Cell Biol. 2009; 187:81–89. [PubMed: 19805630]
40. Pan X, et al. Mechanism of transport of IFT particles in C. elegans cilia by the concerted action of kinesin-II and OSM-3 motors. J Cell Biol. 2006; 174:1035–1045. [PubMed: 17000880]
41. Lord AM, North TE, Zon LI. Prostaglandin E2: making more of your marrow. Cell Cycle. 2007; 6:3054–3057. [PubMed: 18075310]
42. Regan JW. EP2 and EP4 prostanoid receptor signaling. Life Sci. 2003; 74:143–153. [PubMed: 14607241]
43. Youk H, Lim WA. Secreting and sensing the same molecule allows cells to achieve versatile social behaviors. Science. 2014; 343:1242782. [PubMed: 24503857]
44. Haxel BR, Schafer D, Klimek L, Mann WJ. Prostaglandin E2 activates the ciliary beat frequency of cultured human nasal mucosa via the second messenger cyclic adenosine monophosphate. Eur Arch Otorhinolaryngol. 2001; 258:230–235. [PubMed: 11548900]

45. Gross GA, et al. Opposing actions of prostaglandins and oxytocin determine the onset of murine labor. Proc Natl Acad Sci U S A. 1998; 95:11875–11879. [PubMed: 9751758]
46. Loftin CD, et al. Failure of ductus arteriosus closure and remodeling in neonatal mice deficient in cyclooxygenase-1 and cyclooxygenase-2. Proc Natl Acad Sci U S A. 2001; 98:1059–1064. [PubMed: 11158594]
47. Dinchuk JE, et al. Renal abnormalities and an altered inflammatory response in mice lacking cyclooxygenase II. Nature. 1995; 378:406–409. [PubMed: 7477380]
48. Reese J, et al. Coordinated regulation of fetal and maternal prostaglandins directs successful birth and postnatal adaptation in the mouse. Proc Natl Acad Sci U S A. 2000; 97:9759–9764. [PubMed: 10944235]
49. Goetz SC, Liem KF Jr, Anderson KV. The spinocerebellar ataxia-associated gene Tau tubulin kinase 2 controls the initiation of ciliogenesis. Cell. 2012; 151:847–858. [PubMed: 23141541]
50. Becker-Heck A, et al. The coiled-coil domain containing protein CCDC40 is essential for motile cilia function and left-right axis formation. Nat Genet. 2011; 43:79–84. [PubMed: 21131974]
51. Westerfield, M. The Zebrafish Book. Eugene, OR: University of Oregon Press; 2000.
52. Driever W, et al. A genetic screen for mutations affecting embryogenesis in zebrafish. Development. 1996; 123:37–46. [PubMed: 9007227]
53. Zhong TP, Childs S, Leu JP, Fishman MC. Gridlock signalling pathway fashions the first embryonic artery. Nature. 2001; 414:216–220. [PubMed: 11700560]
54. Williams C, et al. Hedgehog signaling induces arterial endothelial cell formation by repressing venous cell fate. Dev Biol. 2010; 341:196–204. [PubMed: 20193674]
55. Higginbotham H, et al. Arl13b-regulated cilia activities are essential for polarized radial glial scaffold formation. Nat Neurosci. 2013; 16:1000–1007. [PubMed: 23817546]
56. Bogard AS, Xu C, Ostrom RS. Human bronchial smooth muscle cells express adenylyl cyclase isoforms 2, 4, and 6 in distinct membrane microdomains. J Pharmacol Exp Ther. 2011; 337:209–217. [PubMed: 21228062]
57. Hoque MT, Cole SP. Down-regulation of Na+/H+ exchanger regulatory factor 1 increases expression and function of multidrug resistance protein 4. Cancer Res. 2008; 68:4802–4809. [PubMed: 18559527]
58. Leggas M, et al. Mrp4 confers resistance to topotecan and protects the brain from chemotherapy. Mol Cell Biol. 2004; 24:7612–7621. [PubMed: 15314169]

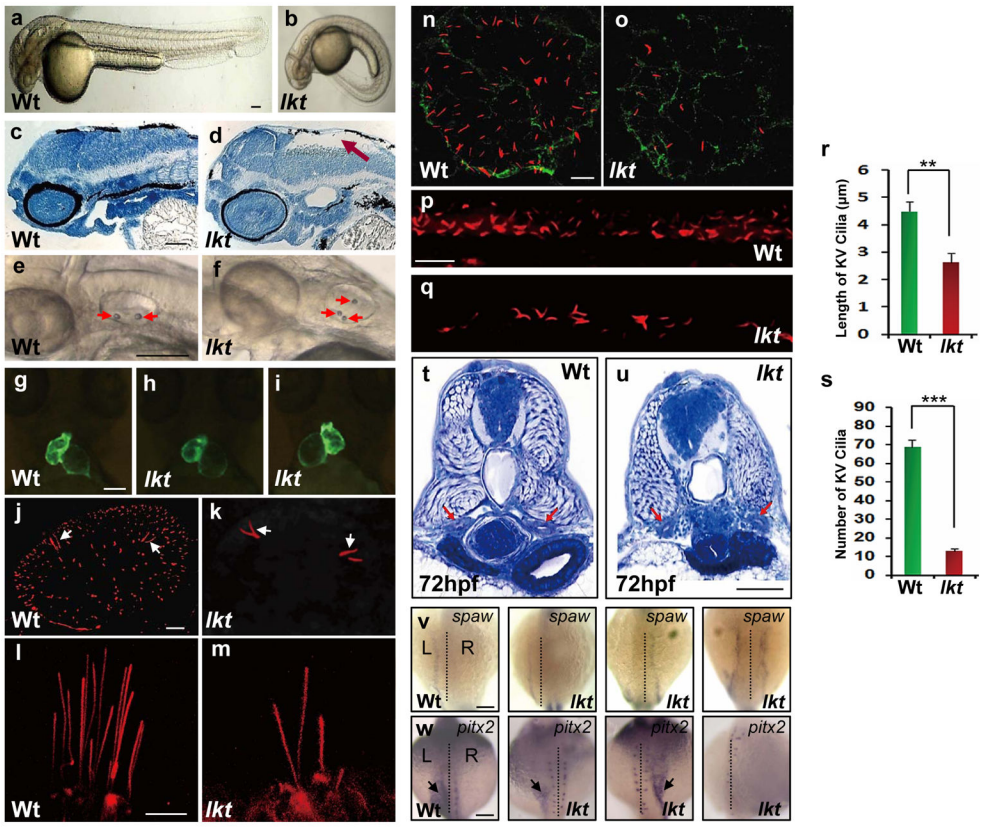

Figure 1. *lkt* mutants exhibit cilia loss and cilia-associated phenotypes

(**a–f**) Lateral views showing a ventrally curved body (b), hydrocephalus (red arrow) (d) and three otoliths (red arrows) (f) in *lkt* mutants compared to wild-type (wt) embryos at 72 hpf (a, c, e). (**g–i**) Cardiac-specific EGFP fluorescence displaying normal right-looped heart in wild-type (wt) *Tg(cmlc2:EGFP)* embryos in ventral view (g). Reversed left-looped heart is present in ~38% of *lkt* mutants (i), and right-looped heart in ~62% of *lkt* mutants (h) at 48 hpf. (**j, k**) Acetylated tubulin staining revealing two clusters of long tether cilia (arrows) and short cilia throughout the otic vesicle in wt embryos at 24 hpf (j). The absence of short cilia and relatively normal tether cilia are observed in the otic vesicle of *lkt* mutants (k). (**l, m**) Acetylated tubulin staining revealing kinocilla loss at the lateral crista of semicircular canals in *lkt* mutants (m) compared to normal kinocilia in wt embryos at 96 hpf (l). (**n, o**) Confocal microscopy images depicting KV cilia (red) and epithelial cells (green) immunostained with anti-acetylated tubulin and anti-αPKC antibodies, respectively, in wt (n), and *lkt* mutant embryos at 13 hpf (o). (**p, q**) Immunostaining of ependymal cell cilia in the spinal canal of wt (p) and in *lkt* mutants (q) at 48 hpf. (**r, s**) KV cilia length and number in wild-type embryos and *lkt* mutants. n = 3 independent experiments, in which 12 total wild-type embryos and 12 total *lkt* mutant embryos were visualized. Graph shows mean ± s.d.; Student's t-test: $^{**}P$ <0.01, $^{***}P$ <0.001. Data are pooled from 3 independent experiments. (**t, u**) Histological sections showing normal pronephric duct development (arrows) without cyst formation in *lkt* mutants compared to wild-type embryos. (**v, w**) *spaw* (v) and *pitx2* (w) expression in LPM showed normal left-sided expression of these genes in wild-type embryos, whereas expression in *lkt* mutants was often randomized. Dotted line denotes the

midline. L=left, R=right. Scale bar: 100 μm (a–i; t, u; v, w). 10 μm (j–q). Statistics source data for Fig. 1r, s can be found in Supplementary Table 2.

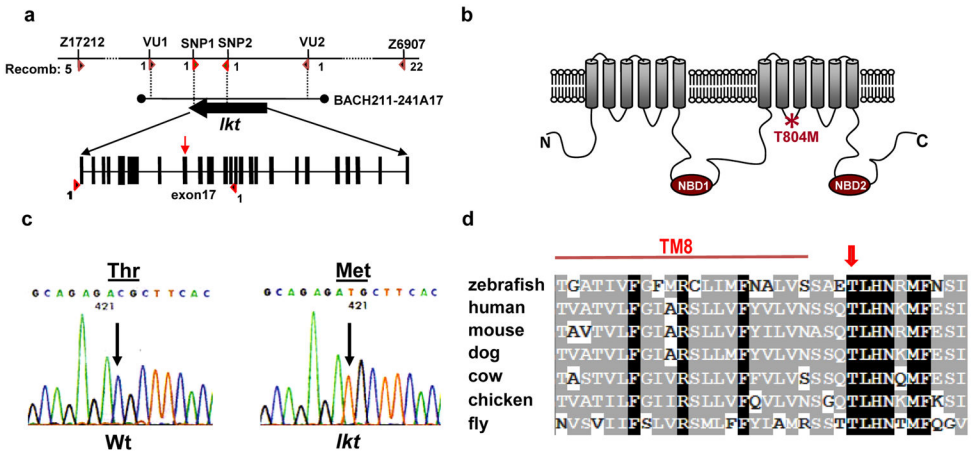

Figure 2. Positional cloning identifies *leakytail* as the ABCC4 transporter.<
br>(**a**) An integrated genetic and physical map of the *lkt* genomic region. Arrowheads indicate recombinants. Red arrow: lkt^{T804M} mutation in exon17. The genomic interval covering the *lkt* mutation was defined by genotyping 1745 mutant embryos (3490 meioses). Z17212, Z6907, VU1, and VU2 are single strand length polymorphisms (SSLP). Single nucleotide polymorphisms (SNP): SNP1, SNP2. (**b**) Schematic diagram of the predicted Lkt/ABCC4 protein secondary structure. The lkt^{T804M} mutation resides within the third cytoplasmic loop connecting transmembrane domain 8 and 9. NBD: nucleotide binding domain. (**c**) Electropherograms of wild-type and *lkt* genomic DNA depicting a C-to-T substitution (arrow). (**d**) Alignment of *lkt*/*abcc4* amino acid sequences across species. Red arrow: conserved threonine. TM8: transmembrane subunit 8.

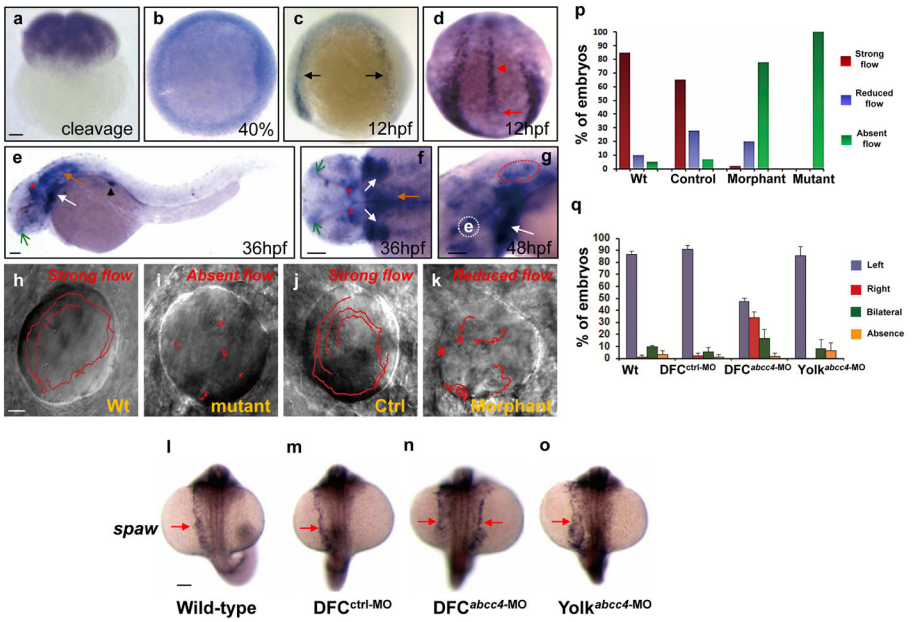

Figure 3. *lkt/abcc4* is expressed during embryonic development and regulates organ laterality in DFC/KV cells

(**a, b**) Whole mount RNA in situ hybridizations revealing ubiquitous *lkt/abcc4* expression at the two-cell stage (a), and the 40%-epiboly stage (b). (**c, d**) At the 6-somite stage (12 hpf), *lkt/abcc4* is expressed in neural crest cells (c; black arrows), the notochord (d; red arrowhead) and KV (d; red arrow). (**e–g**) From 36 hpf onwards, *lkt/abcc4* expression was detected in the olfactory placodes (e and f; green arrows), branchial arches (eg; white arrows), midbrain-hindbrain boundary (e and f; red stars), hindbrain (e and f; brown arrow), pancreas (e; black arrowhead) and the otic vesicle (g; outlined by red circle). e: eye. (**h–k**) Fluorescent bead tracking in the KV revealed that wt embryos (h) and ctrl-MO injected embryos (j) exhibit strong directional fluid flow, whereas flow was either absent or reduced in *lkt* mutants (i) and *lkt/abcc4* morphants (k). (**l–o**) *spaw* expression (arrows) in wt embryos, DFC$^{\text{ctrl-MO}}$, DFC$^{abcc4\text{-MO}}$, and Yolk$^{abcc4\text{-MO}}$ mosaic embryos. (**p**) Percentages of embryos showing strong, reduced or absent KV flow. n = 2 independent experiments. Number of embryos analyzed: Wt=22; Control=19; *lkt* mutant=4; *abcc4* morphant=14. Source data for Fig. 3p can be found in Supplementary Table 1. (**q**) Percentages of DFC$^{abcc4\text{-MO}}$ and control embryos (Wt, DFC$^{\text{ctrl-MO}}$ or Yolk$^{abcc4\text{-MO}}$) showing different *spaw* expression patterns. The percentage of embryos with LR defects is significantly higher in DFC$^{abcc4\text{-MO}}$ embryos than Wt, DFC$^{\text{ctrl-MO}}$ or Yolk$^{abcc4\text{-MO}}$ embryos, but not statistically different among Wt, DFC$^{\text{ctrl-MO}}$ or Yolk$^{abcc4\text{-MO}}$ embryos (Yates corrected Chi-square test, ***$P < 0.0001$, degree of freedom = 1; n = 3 independent experiments in which 104 wild-type embryos, 81 DFC$^{\text{ctrl-MO}}$ injected embryos, 59 DFC$^{abcc4\text{-MO}}$ injected embryo and 33 Yolk$^{abcc4\text{-MO}}$ injected embryos were examined. Control-MO: standard fluorescein-MO. Statistics source data for Fig. 3q can be found in Supplementary Table 2.

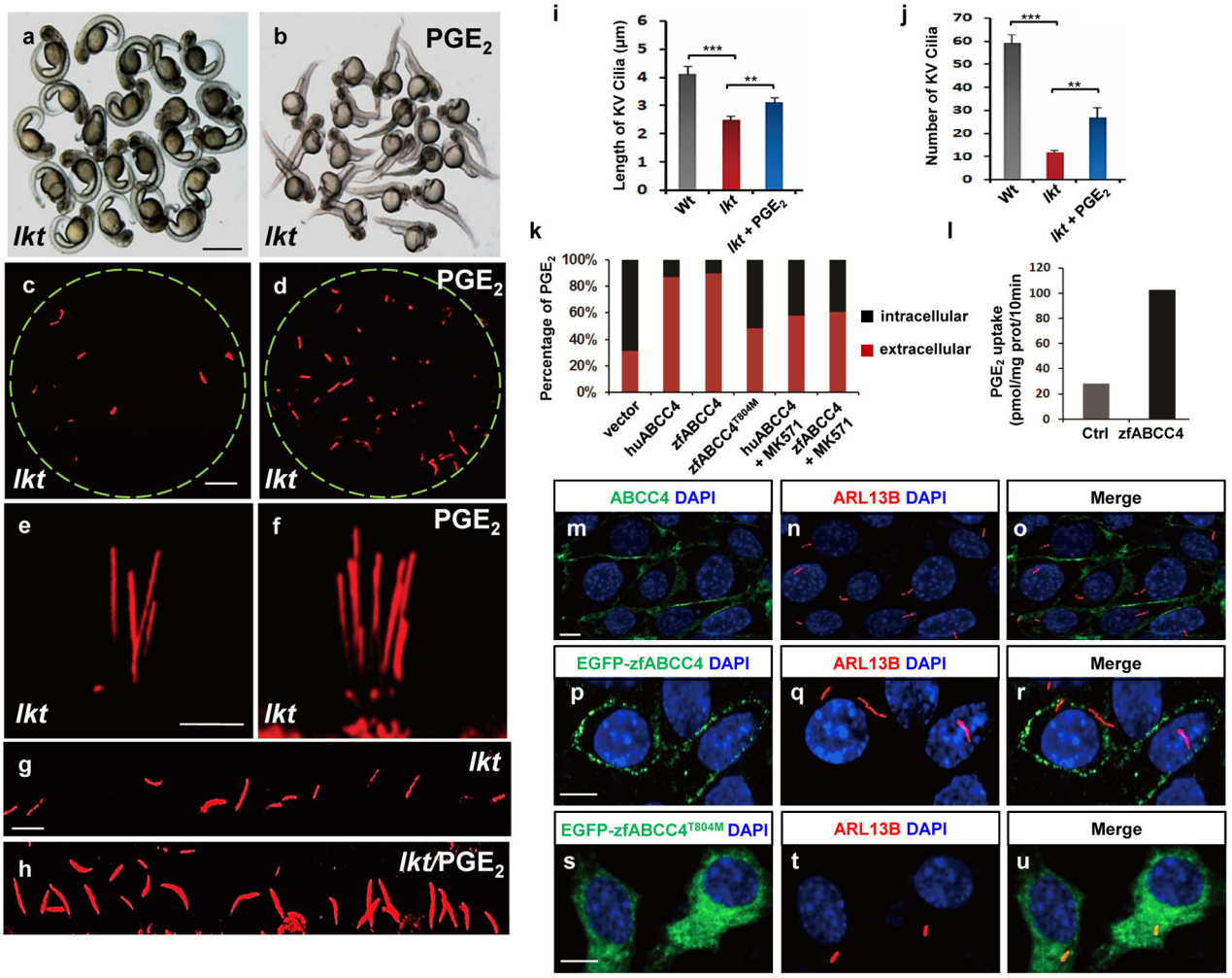

Figure 4. Lkt/ABCC4 exports PGE_2 and regulates ciliogenesis.<

br>(**a, b**) *lkt* mutants with PGE_2 treatment (50 μM; 10–72 hpf) display straight body axes (b; n=34; 86% were rescued) compared to untreated *lkt* mutant embryos (a). (**c, d**) Acetylated tubulin staining showing rescued KV cilia in *lkt* mutants treated with PGE_2 (d; 50 μM; 3–13 hpf; n=12; 75% were rescued) compared to those in untreated *lkt* mutants (c). (**e, f**) Kinocilia loss was partially reversed in *lkt* mutants treated with PGE_2 (f; 50 μM; 24–96 hpf; n=12) compared to those in untreated *lkt* mutants (e). (**g, h**) PGE_2 treatment rescued ependymal cilia loss (50 μM; 10–48 hpf; n=10) in *lkt* mutants (h) compared to those in untreated *lkt* mutants (g). Embryos with *lkt* genotypes but showing abundant cilia and straight axes were scored as rescued mutants. (**i, j**) Bar charts depicting statistical analyses of KV cilia number and length in wt embryos, *lkt* mutants or PGE_2-treated *lkt* mutants Graph shows mean ± s.d.; Student's t-test: $^{**}P$ <0.01, $^{***}P$ <0.001. n = 3 independent experiments in which 12 wt embryos, 12 *lkt* mutants or 12 PGE_2-treated *lkt* mutants were analyzed. (**k**) Lkt/$ABCC4^{T804M}$ transporter disrupts PGE_2 export. Bar charts displaying percentages of intracellular and extracellular PGE_2 in $MEF^{abcc4-/-}$ cells transfected with empty vector, or vectors encoding human ABCC4 (huABCC4), zebrafish ABCC4 (zfABCC4), zebrafish mutant Lkt/$ABCC4^{T804M}$ ($zfABCC4^{T804M}$) as indicated. huABCC4- and zfABCC4-

transfected cells were also treated with MK571. n = 2 independent experiments. (**l**) ATP-dependent uptake of PGE_2 in inside-out membrane vesicles prepared from HEK293T cells expressing zfABCC4 and control vectors. n = 2 independent experiments. (**m–o**) Immunostaining images revealing murine ABCC4 on the plasma cell membrane (green) but not in the cilium (red). (**p–r**) Zebrafish EGFP-ABCC4 protein fusion (EGFP-zfABCC4) was detected on the plasma cell membrane (green) but not in the cilium (red). (**s–u**) Zebrafish EGFP-ABCC4^{T804M} mutant protein fusion (EGFP-zfABCC4^{T804M}) was found in the cytoplasm (green) but not in the cilium (red). Green: EGFP fusions; Red: ARL13B in cilia; Blue: DAPI in nuclei. Scale bar: 1 mm (a, b); 10 μm (c–h); 10 μm (m–u). Statistics source data for Fig. 4i, j, k, l can be found in Supplementary Table 2.

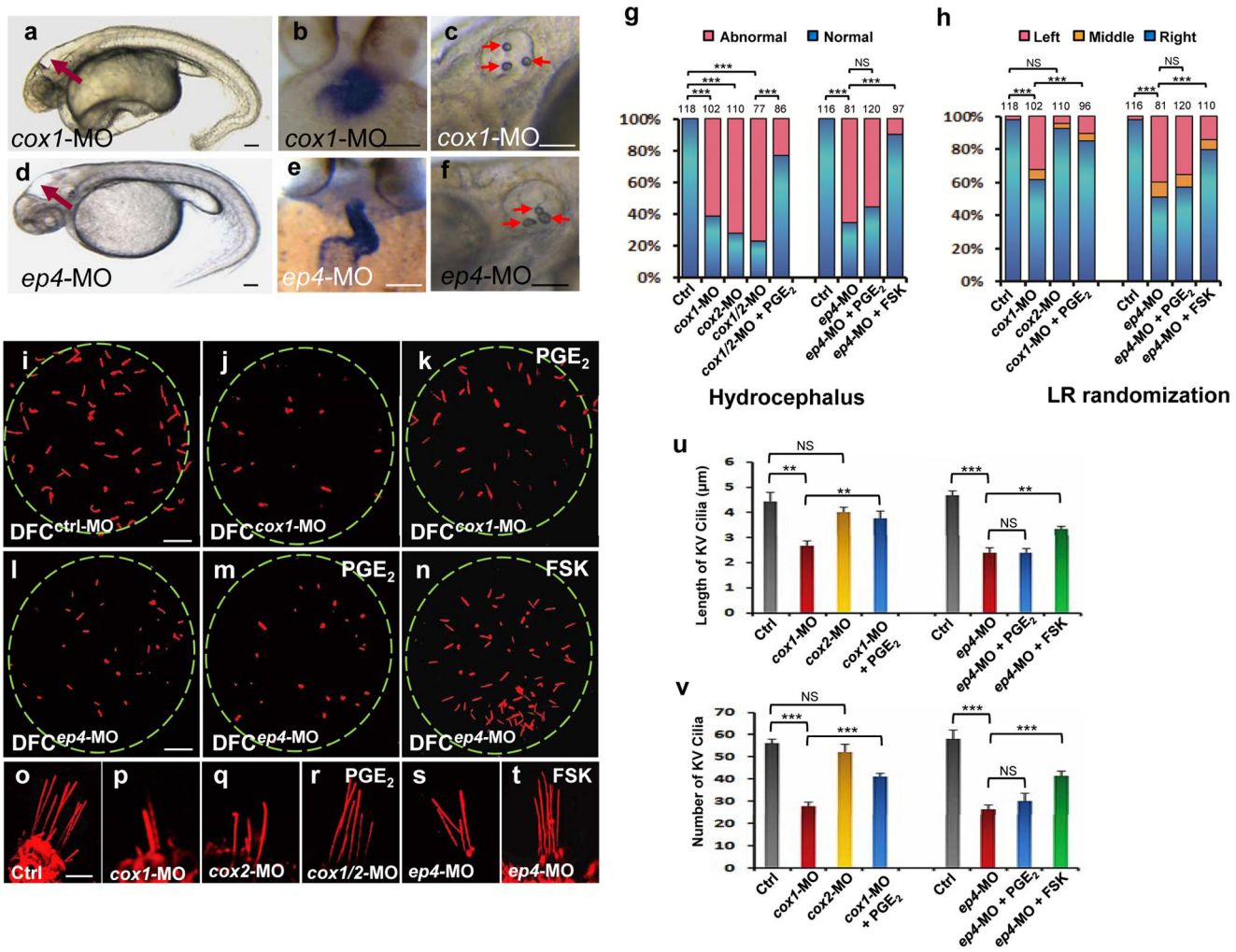

Figure 5. COX-EP4 signaling pathway is required for ciliogenesis.<

br>(**a–c**) Embryos injected with *cox1*-MO (8 ng) exhibited a curved body axis, hydrocephalus (a; arrow), reverse-looped heart (b) and three otoliths (c; arrows). (**d–f**) *ep4*-MO-injected embryos (1 ng) featured a curved body axis, hydrocephalus (d; arrow), a reversed looped-heart and three otoliths (f; arrows). (**g–h**) Percentages of embryos with phenotypes grouped in hydrocephalus (g) and LR randomization (h). PGE_2 treatment (50 μM) of *cox1/2* morphants and *cox1* morphants partially rescued hydrocephalus (10–72 hpf) and LR randomization (3–24 hpf). Treating *ep4* morphants with forskolin (FSK; 50 μM) but not PGE_2 rescued hydrocephalus and LR randomization. Ctrl: Ctrl-MO-injected embryos. The total numbers of embryos pooled from n = 3 independent experiments are indicated on the top of each bar. Yates corrected Chi-square test, $^{***}P < 0.0001$, degree of freedom =1. NS: Not significant. (**i–k**) Acetylated tubulin staining revealed normal KV cilia in $DFC^{ctrl\text{-}MO}$ embryos (i), cilia loss in $DFC^{cox1\text{-}MO}$ embryos (j) (8 ng; n=12), and restored cilia in PGE_2-treated $DFC^{cox1\text{-}MO}$ embryos (k) (50 μM; 3–13 hpf; n=12). (**l, m**) KV cilia loss in $DFC^{ep4\text{-}MO}$ embryos (1 ng; n=11), PGE_2-treated $DFC^{ep4\text{-}MO}$ embryos (50 μM; 3–13 hpf; n=13). (**n**) Rescued KV cilia loss in $DFC^{ep4\text{-}MO}$ embryos treated with FSK (50 μM; 3–13 hpf; n=11). (**o–q**) Kinocilia loss in embryos injected with *cox1*-MO (8 ng; n=15) (p) or

cox2-MO (q) (8 ng; n=18), compared with controls (o). (**r**) PGE_2 treatment rescued *cox1/2*-morphants (50 μM; 24–96 hpf; n=12). (**s**) *ep4*-MO-injected embryos (1 ng) exhibited kinocilia loss (s) (n=14); (**t**) FSK treatment rescued kinocilia loss in *ep4* morphants (50 μM; 24–96 hpf; n=10). (**u, v**) Quantification of KV cilia number and length in $DFC^{ctrl\text{-}MO}$, $DFC^{cox1\text{-}MO}$, $DFC^{cox2\text{-}MO}$, PGE_2–treated $DFC^{cox1\text{-}MO}$ embryos, and in $DFC^{ctrl\text{-}MO}$, $DFC^{ep4\text{-}MO}$, PGE_2–treated $DFC^{ep4\text{-}MO}$, FSK-treated $DFC^{ep4\text{-}MO}$ embryos. Error bar shows mean ± s.d.; Student's t-test: $^{**}P < 0.01$, $^{***}P < 0.001$. NS: Not significant ($P > 0.05$). n = 3 independent experiments in which 12 $DFC^{ctrl\text{-}MO}$, 12 $DFC^{cox1\text{-}MO}$, 12 $DFC^{cox2\text{-}MO}$, 12 PGE_2–treated $DFC^{cox1\text{-}MO}$ embryos (left bar graphs), and 12 $DFC^{ctrl\text{-}MO}$, 11 $DFC^{ep4\text{-}MO}$, 13 PGE_2–treated $DFC^{ep4\text{-}MO}$ and 11 FSK-treated $DFC^{ep4\text{-}MO}$ embryos (right bar graphs) were analyzed. Scale bar: 100 μm (a–f); 10 μm (i–t). Statistics source data for Fig. 5g, h, u, v can be found in Supplementary Table 2.

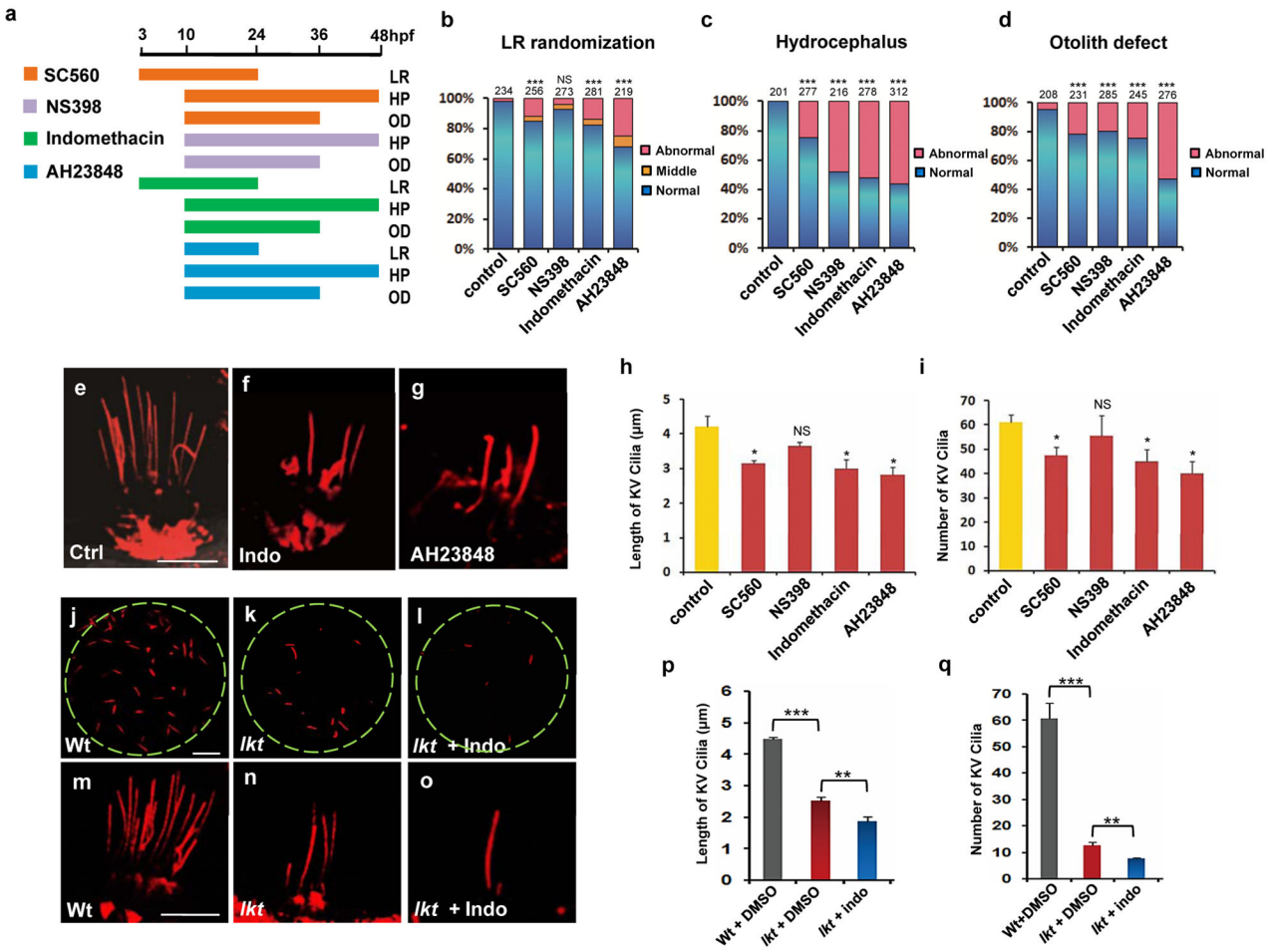

Figure 6. Inhibition of the COX-EP4 signaling pathway using pharmacological agents leads to ciliogenesis defects.<

br>(**a**) A diagram depicting the timeframe of pharmacological treatment for SC560 (125 uM, Cox1 inhibitor,), NS398 (125 uM, Cox2 inhibitor), Indomethacin (150 uM, Cox1 + Cox2 inhibitor), AH23848 (10 uM, Ep4 inhibitor). The resulting phenotypes are listed to the right: LR: Left-right randomization (3–24 hpf for SC560, H238480; 10–24 hpf for AH23848). HP: Hydrocephalus (10–48 hpf). OD: Otolith defect (10–36 hpf). (**b–d**) Bar charts displaying percentages of embryos with cilia-associated phenotypes following chemical treatments. Left-right randomization (b), Hydrocephalus (c) and otolith defects (d) are shown. Control: DMSO (0.1%)-treated embryos. The total numbers of embryos pooled from n = 3 independent experiments are indicated on the top of each bar. Yates corrected Chi-square test, $^{***}P < 0.0001$, degree of freedom = 1. NS: Not significant. (**e–g**) Acetylated tubulin immunostaining showing kinocilia loss in Indomethacin- (150 uM; 10–48 hpf; n=12) and AH23848-treated (10 uM; 10–48 hpf; n=15) embryos at 96 hpf, compared with DMSO-treated embryos. (**h, i**) Bar graphs depicting KV cilia length and number in embryos treated with SC560 (100 uM), NS398 (100 uM), Indomethacin (150 uM) and AH23848 (10 uM) compared with 0.1% DMSO-treated controls from 3 to 13 hpf. Error bar represents mean ± s.d.; Student's t-test: $^{*}P$ <0. 01. NS: Not significant. n = 3 independent experiments in which 12 DMSO- treated, 12 SC560-treated, 9 NS398-treated, 10 indomethacin-treated and 12

AH23848-treated embryos were analyzed. (**i-l**) Acetylated tubulin staining reveals reduction of KV cilia in *lkt* mutants treated with Indomethacin (150 uM; 3–14 hpf; n=10) compared to DMSO-treated *lkt* mutants (0.1%; 3–14 hpf; n=12) and wild-type embryos. (**m–o**) Acetylated tubulin staining reveals kinocilia loss in *lkt* mutants treated with Indomethacin (150 uM; n=12; 10–48 hpf) compared with DMSO-treated *lkt* mutants (0.1%; n=12;10–48 hpf) and wild-type embryos at 96 hpf. (**p, q**) Quantification of KV cilia length and number in DMSO-treated wild-type embryos, DMSO-treated *lkt* mutants, Indomethacin-treated *lkt* mutants. Student's t-test: $^{***}P$ <0.001; Error bar represents mean ± s.d.; n = 3 independent experiments in which 12 DMSO-treated WT embryos, 12 DMSO-treated *lkt* mutants and 10 Indomethacin-treated *lkt* mutants were analyzed. Scale bar: 10 μm (e–g; j–l; m–o). Statistics source data for Fig. 6b–d; h, I; p, q can be found in Supplementary Table 2.

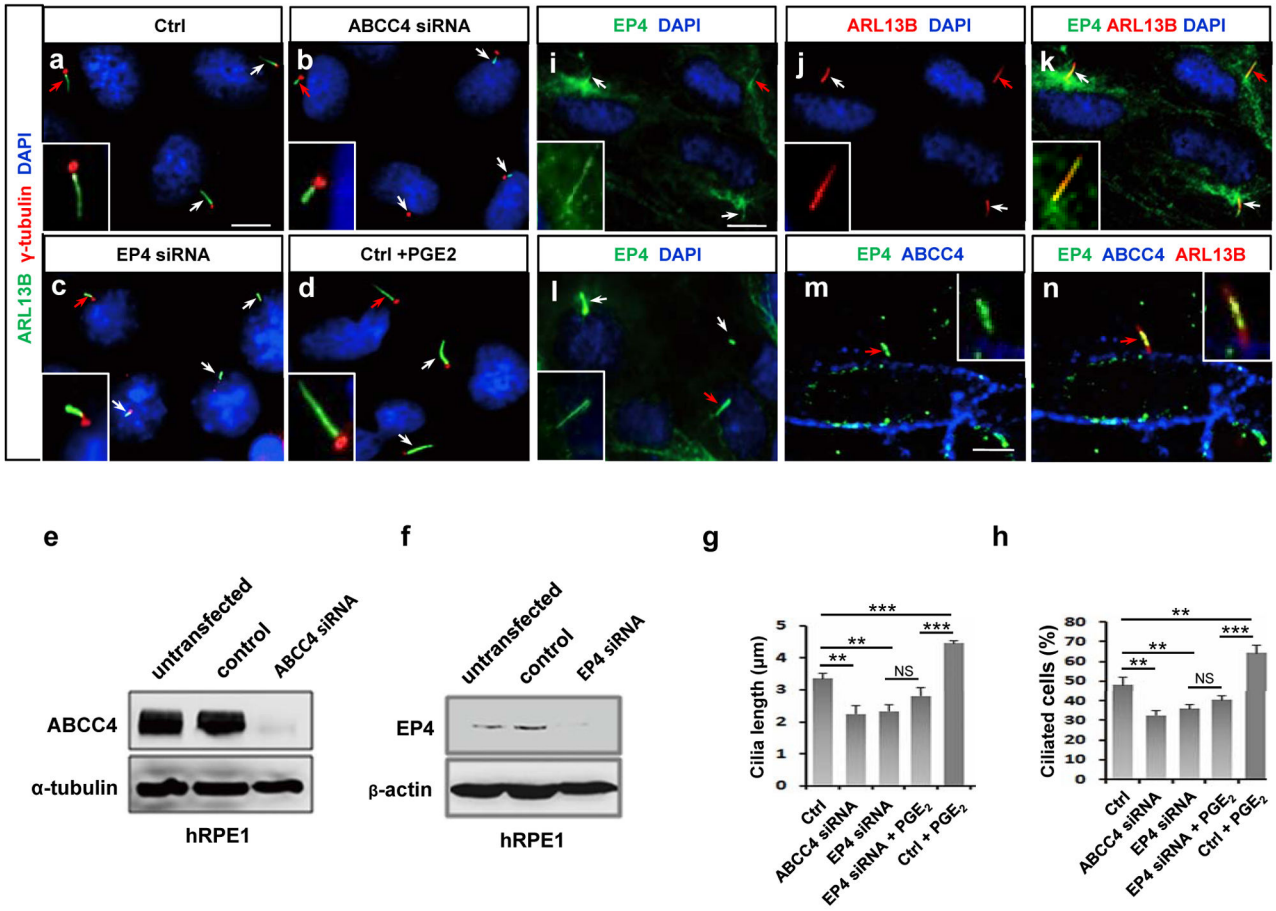

Figure 7. Lkt/ABCC4-mediated PGE_2 signaling promotes ciliogenesis in mammalian cells

(**a–d**) Immunostaining analyses showing individual cilia in hRPE1 cells treated with control siRNA (100 nM), ABCC4 siRNA (100 nM), EP4 siRNA (100 nM) or PGE_2 (10 μM; 12 h). Insets reveal high-magnification images of cilia (red arrows). Green: ARL13B for cilium; Red: γ-tubulin for centrosome; Blue: DAPI; Arrow: cilium. (**e, f**) Immunoblot analysis showing ABCC4 or EP4 protein levels in hRPE1 cells transfected with control siRNA, ABCC4 siRNA or EP4 siRNA. (**g, h**) Statistical analyses of average length of cilia and percentages of ciliated cells in hRPE1 cells transfected with control siRNA (357), ABCC4 siRNA (541), EP4 siRNA (479), EP4 siRNA plus PGE_2 treatment (352), or control siRNA plus PGE_2 treatment (313). Cell numbers (provided in parentheses) for each experiment are pooled from n= 3 independent experiments. Error bar represents mean ± s.d.; Student's t-test: $^{**}P < 0.01$, $^{***}P < 0.001$. **(i–k)** Immunostaining for EP4 (i), ARL13B (j) or the co-localization of EP4 with ARL13B in the cilium (k) in hRPE1 cells. (**l**) Localization of EP4 in the cilium in IMCD3 cells. (**m–n**) EP4 localizes to the cilium, whereas ABCC4 localizes on the plasma membrane in the same hRPE1 cell. Insets show high-magnification images of cilia (red arrows). Green: EP4; Red: ARL13B; Blue: DAPI or ABCC4 (i–l) or ABCC4 (m–n); Arrow: cilium. Scale bar: 10 μm (a–d; i–l); 15 μm (m, n). Statistics source data for Fig. 7g, h can be found in Supplementary Table 2.

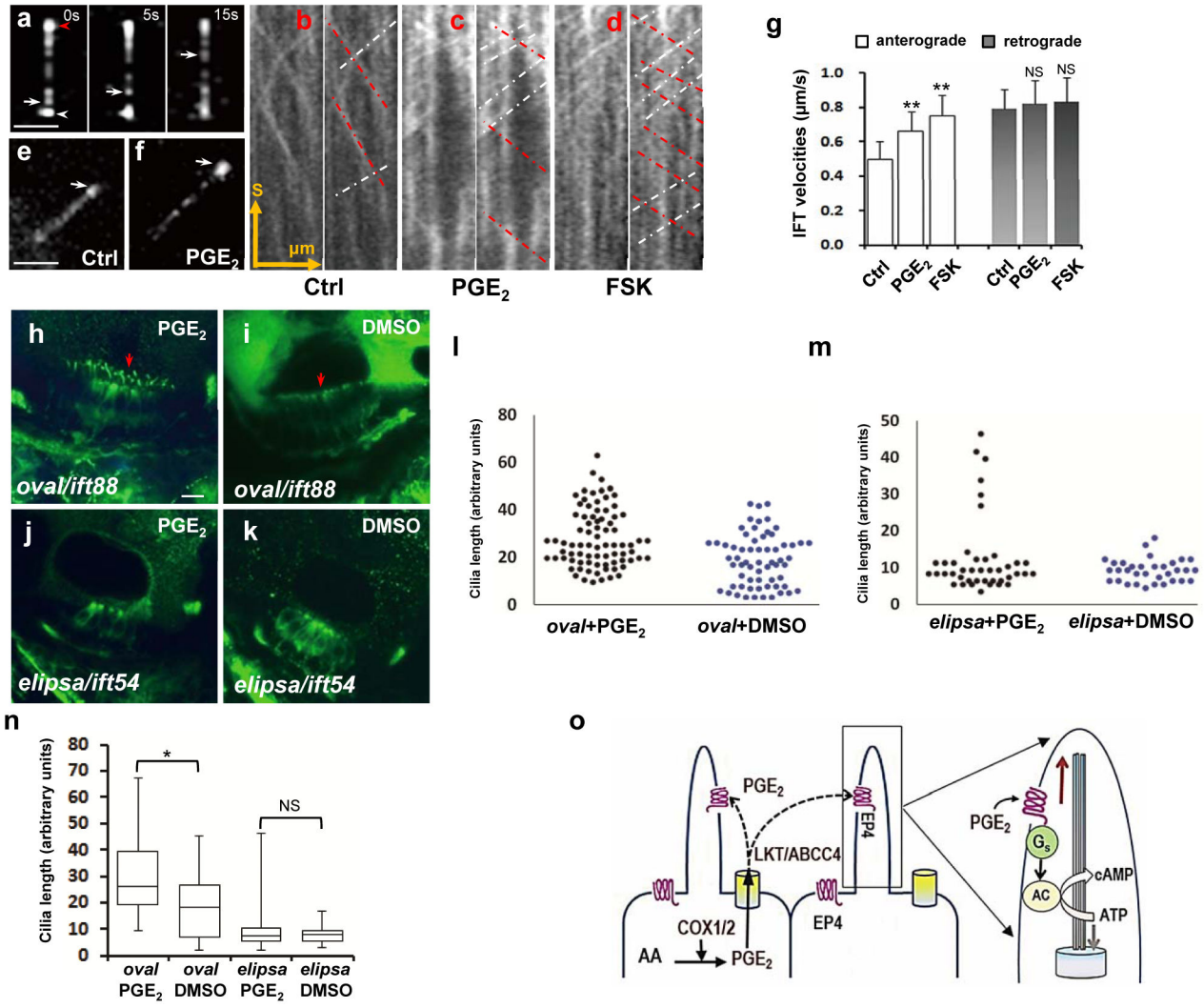

Figure 8. PGE_2 signaling increases anterograde velocity of IFT

(**a**) Time-lapse images illustrating changes in the positions of IFT88-EYFP particles along the ciliary axoneme. White arrow: particle position. Red arrowhead: cilium tip. White arrowhead: Basal body. (**b–d**) Time- lapse images were assembled into kymographs. Red and white dotted lines indicate anterograde and retrograde transport, respectively. Distance scale bar (horizontal): 4 μm. Time scale bar (vertical): 10 sec. (**e, f**) The accumulation of fluorescent IFT88 was observed at cilia tips in PGE_2-treated cells (f) compared to control cells (e). Arrow: cilium tip. (**g**) Bar graph depicting IFT velocities. Sample sizes for the measurements of the anterograde and reterograde velocities of individual IFT88-EYFP particles are as follows: 55 anterograde and 52 retrograde particles for control cells; 51 anterograde and 53 retrograde particles for PGE_2-treated cells; 38 anterograde and 35 retrograde particles for FSK-treated cells. Student's t-test, mean ± s.d. $^{**}P < 0.01$. n = 5 independent experiments. (**h–k**) Acetylated tubulin staining of cilia (arrows) at 3 dpf in the anterior macula of *oval/ift88* (h, i) and *elipsa/ift54* (j, k) mutants subjected to PGE_2 (50–70 uM PGE_2; 24 to 72 hpf) or control (0.01% DMSO) treatments as indicated. (**l–n**) Scatter diagram displays individual cilium length in the anterior macula of PGE_2- and DMSO-

treated *oval/ift88* mutants (l), as well as PGE_2- and DMSO-treated *elipsa/ift54* embryos (m). Cilia from PGE2-treated *oval/ift88* embryos (80), DMSO-treated *oval/ift88* embryos (63), PGE2-treated *elipsa/ift54* embryos (42) and DMSO-treated *elipsa/ift54* embryos (33) were analyzed. The results were subjected to Mann-Whitney *U* Tests ($^*P < 0.05$; total number of embryos pooled from n = 3 independent experiments presented in parentheses), and presented as boxplots (n). (**o**) A model of prostaglandin signaling in ciliogenesis. PGE_2 is synthesized by COX1 and COX2 and exported via the Lkt/ABCC4 transporter on the cell membrane. Released PGE_2 binds to the EP4 receptor on the cilium, resulting in the activation of Gs and adenylate cyclase to increase cAMP, thereby increasing the anterograde IFT and enhancing ciliogenesis. Scale bar: 5 μm (a, e, f); 10 μm (h–k). Statistics source data for Fig. 8n can be found in Supplementary Table 2. Uncropped images of the immunoblots are shown in Supplementary Figure 9.